HETEROCYCLES, Vol. 101, No. , 2020, pp. -. © 2020 The Japan Institute of Heterocyclic Chemistry
Received, 26th June, 2019, Accepted, 13th August, 2019, Published online, 2nd October, 2019
DOI: 10.3987/COM-19-S(F)30

MECHANISTIC STUDIES OF NICKEL(II)-CATALYZED DIRECT ALCOHOLYSIS OF 8-AMINOQUINOLINE AMIDES

Hiroyuki Morimoto,* Walaa Akkad, Toru Deguchi, and Takashi Ohshima*

Graduate School of Pharmaceutical Sciences, Kyushu University, Fukuoka 812-8582, Japan. E-mail: hmorimot@phar.kyushu-u.ac.jp
ohshima@phar.kyushu-u.ac.jp

Abstract – This paper describes the mechanistic aspects of nickel(II)-catalyzed direct alcoholysis of 8-aminoquinoline amides. Kinetic experiments suggested that the nickel(II) catalyst existed in an oligomeric form in the resting state, and the 8-aminoquinoline generated after cleavage coordinated to the nickel(II) catalyst to decelerate the reaction. In addition, density functional theory calculations revealed that the reactions proceeded via the intermediate with *N*,*N*,*O*-tridentate coordination of 8-aminoquinoline amides to the nickel(II) metal center, and that the alcoholysis reaction did not involve deprotonation of the N–H bond of 8-aminoquinoline amides, in contrast to the proposed mechanism for C–H bond functionalization reactions of 8-aminoquinoline amides.

INTRODUCTION

Catalytic alcoholysis of amides is an efficient method for directly transforming amides into more useful esters. The development of such reactions remains a formidable challenge, however, due to the low reactivity of amides and alcohols[1] as well as the thermodynamic stability of the amides relative to the esters, and only a handful of reactions have been reported in the literature.[2–4] In addition, to the best of our knowledge, chemoselective alcoholysis of the directing group amides used in C–H functionalization reactions has not been reported, although it could enhance the transformation of directing-group amides.[5] To this end, and consistent with our ongoing interests in amide chemistry,[6] we previously reported nickel(II)-catalyzed direct chemoselective alcoholysis of 8-aminoquinoline amides (Scheme 1).[7] This reaction allowed for chemoselective cleavage of 8-aminoquinoline amides in the presence of a range of functional groups including related amide moieties, and the reaction was applied to a range of actual products of C–H functionalization reactions.[8]

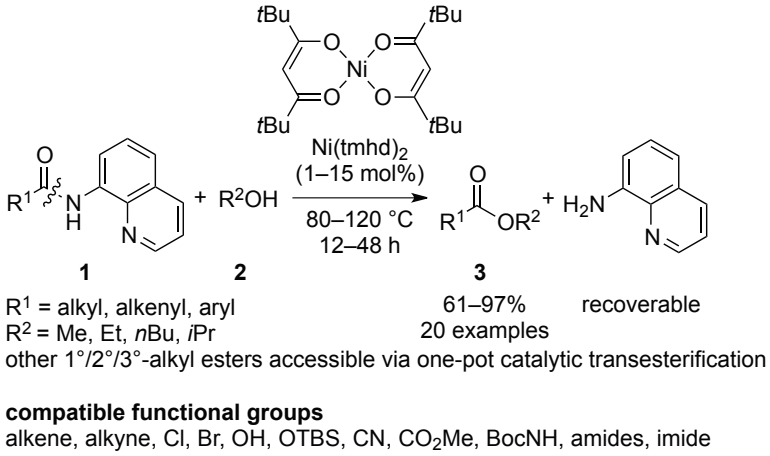

Scheme 1. Nickel(II)-Catalyzed Direct Chemoselective Alcoholysis of 8-Aminoquinoline Amides

Although the reaction development was successful, questions remained in our previous report. In particular, the reaction mechanism was unclear and only a speculative mechanistic picture was provided with limited experimental information (Scheme 2). In addition, the proposed mechanism was inconsistent with the experimental result that *N*-Me-substituted 8-aminoquinoline amide also reacted under the reaction conditions to give esters,[7] while deprotonation of the N–H moiety was involved in our previously proposed catalytic cycle such as intermediates **A** and **B**.

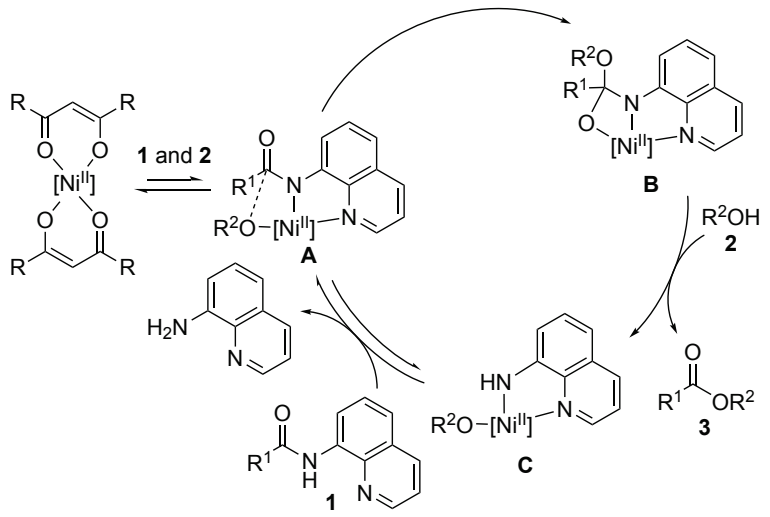

Scheme 2. Previously Proposed Mechanism

To better understand the reaction mechanism of the nickel(II)-catalyzed alcoholysis, we performed additional experimental and computational studies. First, kinetic experiments were performed to clarify the nature of the catalytic cycle. Second, a computational study was implemented to elucidate the detailed information of the reaction mechanism. Below, we describe these results and propose a revised reaction mechanism.

RESULTS AND DISCUSSIONS

1. Kinetic Experiments. First, we performed kinetic experiments to experimentally clarify the reaction mechanism. Using 8-aminoquinoline amide **1a** and methanol (**2a**) as the model substrate, loading of the optimal nickel(II) catalyst $Ni(tmhd)_2$ was increased from 2.5 mol% to 10 mol% (Table 1). As 1 h after starting the reaction, the reaction had a positive order in $[Ni(tmhd)_2]_0$, but the order was less than unity because the concentration of **3a** did not double with a doubling of catalyst loadings.

Table 1. Kinetics of the Alcoholysis of Amide **1a** with Different Concentrations of $Ni(tmhd)_2$[a]

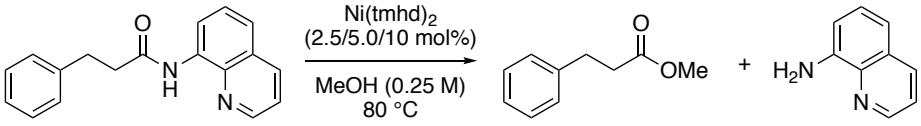

1a **3a**

$Ni(tmhd)_2$ (mol%)	2.5	5.0	10
$[Ni(thmd)_2]_0$ (M)	0.00625	0.0125	0.025
[**1a**]$_0$ (M)	0.25	0.25	0.25
time (h)	[**3a**] (M)[b]	[**3a**] (M)[b]	[**3a**] (M)[b]
0.33	0.018	–	0.036
0.5	–	0.037	–
1	0.042	0.053	0.067
3	0.086	0.103	0.116
9	0.149	0.175	0.178
24	0.196	0.217	0.223
72	0.218	0.233	0.224

[a]The reaction was performed at 0.25 mmol scale of **1a** in MeOH (0.25 M). [b]Concentration of **3a** was determined by ^{1}H NMR analysis of the crude mixture.

To clarify the rate dependency for $Ni(tmhd)_2$, we utilized a graphical method to determine the order in the catalyst (Figure 1).[9] On the basis of graphs with different values of the catalyst order *n*, the data points of each run overlapped most effectively when $n = 0.5$ was applied, while the curves did not overlap when $n = 0$ or 1 was used. These results indicated that the order in $Ni(tmhd)_2$ was approximately 0.5th, suggesting that the higher order nickel complex is present as an off-cycle species in the reaction mixture.[9]

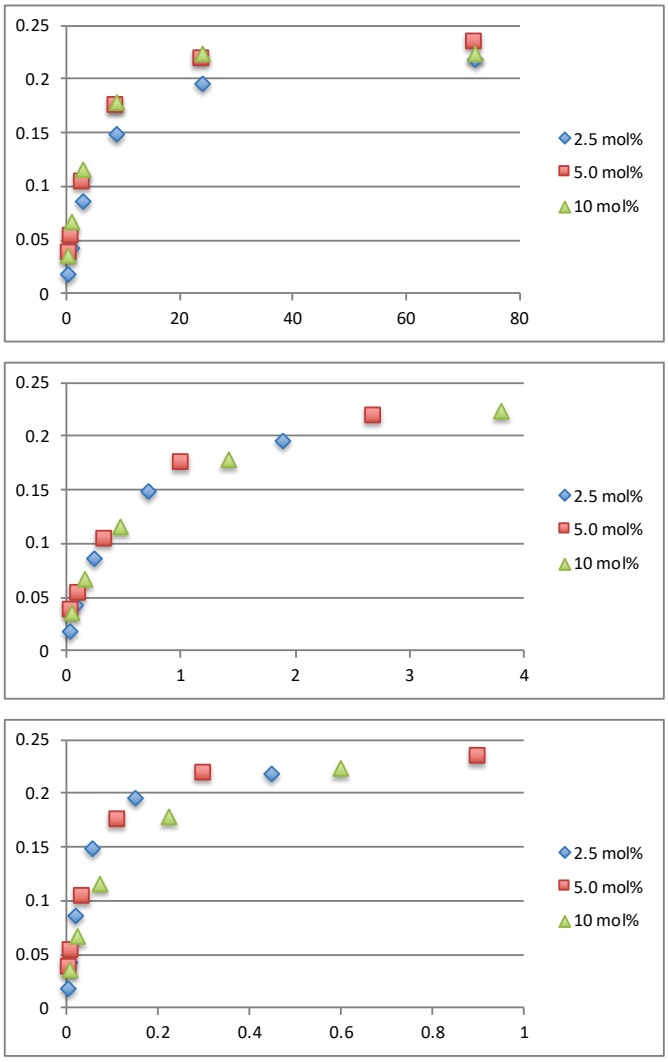

Figure 1. Graphical analysis of the order in the catalyst $Ni(tmhd)_2$. n = 0 (top), 0.5 (middle), and 1 (bottom) was applied with $t[Ni(tmhd)_2]_T^n$ as X-axis and [**3a**] as Y-axis, where t is time (h) and n is the order of $Ni(tmhd)_2$.

Next, the concentration dependency of 8-aminoquinoline amide **1a** was evaluated (Table 2). At 1 h, the initial reaction rate exhibited no significant dependency on $[\mathbf{1a}]_0$, suggesting that the Ni(II) catalyst was saturated with **1a** at the initial stage of the reaction. In addition, analysis of the reaction progress under the pseudo-same [e] conditions[10] with appropriate time-scale adjustments[11] suggested that the reaction decelerated as the reaction proceeded, because the curves with different concentration of $[\mathbf{1a}]_0$ did not overlap and a faster reaction rate was observed at the initial stage of the reaction for the time-adjusted data points (Figure 2). These findings suggested that the 8-aminoquinoline that was generated as the reaction progressed had detrimental effects on the reactivity.

Table 2. Kinetics of the Alcoholysis of Amide **1a** with Different Initial Concentrations of **1a**[a]

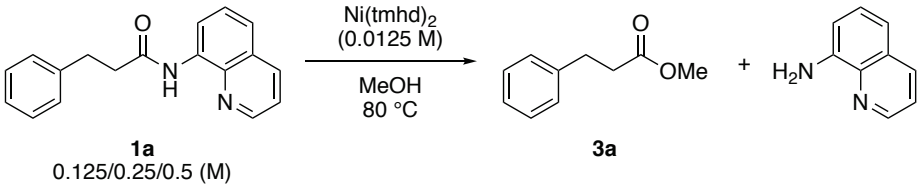

1a
0.125/0.25/0.5 (M)

3a

$[Ni(tmhd)_2]_0$ (M)	0.0125	0.0125	0.0125
$[\mathbf{1a}]_0$ (M)	0.125	0.25	0.5
time (h)	[**3a**] (M)	[**3a**] (M)	[**3a**] (M)
0.33	0.019	–	0.027
0.5	–	0.037	–
1	0.040	0.053	0.049
3	0.072	0.103	0.109
9	0.101	0.175	0.197
24	0.115	0.217	0.301
72	0.119	0.233	0.374

[a]The reaction was performed at 0.125/0.25/0.50 mmol scale of **1a** in MeOH (1 mL). [b]Concentration of **3a** was determined by ^{1}H NMR analysis of the crude mixture.

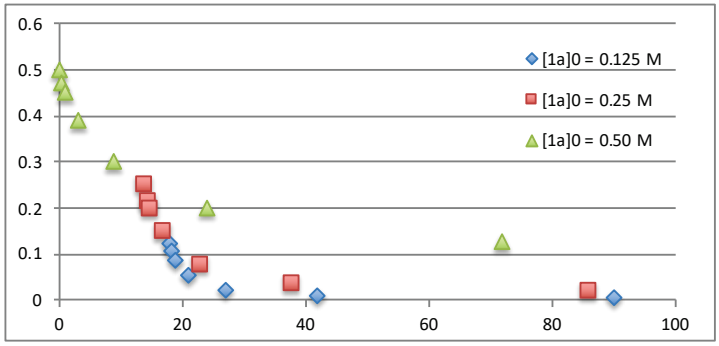

Figure 2. Reaction progress analysis under pseudo-same [*e*] conditions with time (h) as X-axis and [**1a**] as Y-axis. Time-scale adjustment of +14 (h) and +18 (h) was applied for the data points of $[\mathbf{1a}]_0$ = 0.25 (M) and $[\mathbf{1a}]_0$ = 0.125 (M), respectively.

To clarify the effects of the generated 8-aminoquinoline, we next investigated the concentration dependency of the 8-aminoquinoline ($QuinNH_2$) (Table 3). Kinetic experiments revealed that the added 8-aminoquinoline negatively affected the reactivity, and –0.9th order in $[QuinNH_2]$ was obtained from the initial rates. The result was consistent with our previous experimental results, in which the addition of 1 equivalent of 8-aminoquinoline retarded the reaction in the presence of 20 mol% of $Ni(acac)_2$ as a catalyst, as well as with our previously proposed mechanism that 8-aminoquinoline reversibly coordinated to the nickel catalyst.[7]

Table 3. Kinetics of the Alcoholysis of Amide **1a** with Different Initial Concentrations of 8-Aminoquinoline ($QuinNH_2$)[a]

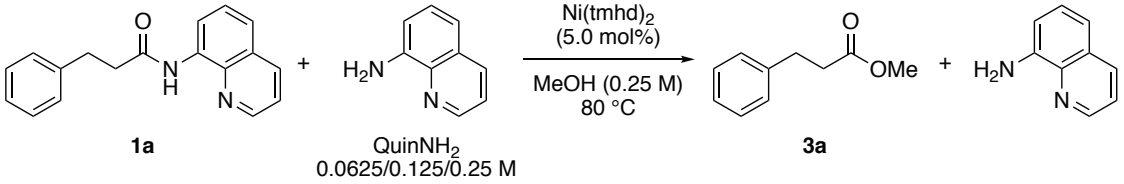

1a $QuinNH_2$ 0.0625/0.125/0.25 M **3a**

$[Ni(tmhd)_2]_0$ (M)	0.0125	0.0125	0.0125
$[\mathbf{1a}]_0$ (M)	0.25	0.25	0.25
$[QuinNH_2]_0$ (M)	0.0625	0.125	0.25
time (h)	[**3a**] (M)	[**3a**] (M)	[**3a**] (M)
0.33	0.0041	0.0011	0.0010
1	0.0104	0.0044	0.0016
3	0.0229	0.0171	0.0060
9	0.0675	0.0362	0.0178
24	0.1164	0.0771	0.0417
72	0.1780	0.1245	0.0733
$d[\mathbf{3a}]/dt$ (M/h)	0.00688	0.00607	0.00197
$\ln[QuinNH_2]_0$	–2.77	–2.08	–1.39
$\ln(d[\mathbf{3a}]/dt)$	–4.98	–5.10	–6.23

[a]The reaction was performed at 0.25 mmol scale of **1a** in MeOH (0.25 M). [b]Yield of **3a** was determined by ^{1}H NMR analysis of the crude mixture.

2. Computational Investigation. With the above experimental results in hand, we next implemented a computational study to clarify the details of the reaction mechanism. We performed density functional theory calculations using Gaussian 16 revision A03;[12] the geometry optimized using B3LYP functional[13] with a 6-31G(d) basis set for all the atoms, and the Ni complexes were treated as a triplet spin state for one Ni atom and a quintet spin state for two Ni atoms. After optimizing the structures, frequency calculations were performed at the same level of theory to confirm that the obtained structures were at either a stationary point (no imaginary frequencies) or a transition state (one imaginary frequency). Intrinsic reaction coordinate calculations were performed for each transition state structure to confirm that the transition state connected the reaction pathway between the starting materials and the products or intermediates. Thermal corrections to the Gibbs energy at 298.15 K were computed by frequency calculations at the level of geometry optimization, and the concentration was adjusted from 1 atm to 1 M (24.465 atm) with a correction factor $RT\ln(0.08206T)$ for each structure, where R is the gas constant (1.987×10^{-3} kcal mol^{-1} K^{-1}) and T is temperature (298.15 K).[14] In addition, the concentration effects of MeOH (24.72 M) were taken into account with a correction factor $RT\ln([MeOH])$ for an explicit MeOH molecule.[15] Single point energy calculations for the optimized geometry were performed using M06 functional[16] with 6-311+G(d,p) basis set for all the atoms using an SMD solvation model (MeOH).[17]

To explain the observed experimental results, we computationally evaluated the thermodynamics of three reactions using 8-aminoquinoline amide **1b**, MeOH (**2a**), and Ni(tmhd)$_2$ (Scheme 3). First, the thermodynamics of the alcoholysis reaction were evaluated without considering the concentration effects of MeOH mentioned above, and the Gibbs energy ($\Delta G°$ = +0.26 kcal mol^{-1}) was obtained (equation 1). Although the Gibbs energy of the reaction was slightly uphill, the equilibrium under the standard reaction conditions could reach 99% conversion of **1b** when excess amounts of MeOH were present as solvent (24.72 M), consistent with the experimental observations. Second, the thermodynamic preference of the formation of dimeric nickel complexes was evaluated to account for the observed rate dependency for Ni(tmhd)$_2$ (equation 2). As a result, formation of the dimeric nickel complex [Ni(tmhd-κ*O*,*O*)(μ-OMe)(MeOH)$_2$]$_2$ (**I**) was thermodynamically more favorable than the starting materials ($\Delta G°$ = –5.1 kcal mol^{-1}), consistent with the observed 0.5th order of the nickel catalyst if a monomeric nickel catalyst was the active species.[9] Third, complexation of the 8-aminoquinoline amide **1b** to the nickel catalyst was evaluated (equation 3), and formation of the complex [Ni(tmhd-κ*O*,*O*')(**1b**-κ*N*,*N*')(MeOH)$_2$] (**II**) was energetically favored ($\Delta G°$ = –2.2 kcal mol^{-1}), consistent with the negligible initial rate dependency for the concentration of 8-aminoquinoline amide **1a** observed during the experimental kinetic study because the nickel metal was saturated with the coordinated 8-aminoquinoline amide at the initial stage of the reaction. Although many more possible complexes should be considered to understand the entire reaction space,[18] these results suggest that the present computational method is appropriate for evaluating the thermodynamics of nickel-catalyzed alcoholysis reactions.

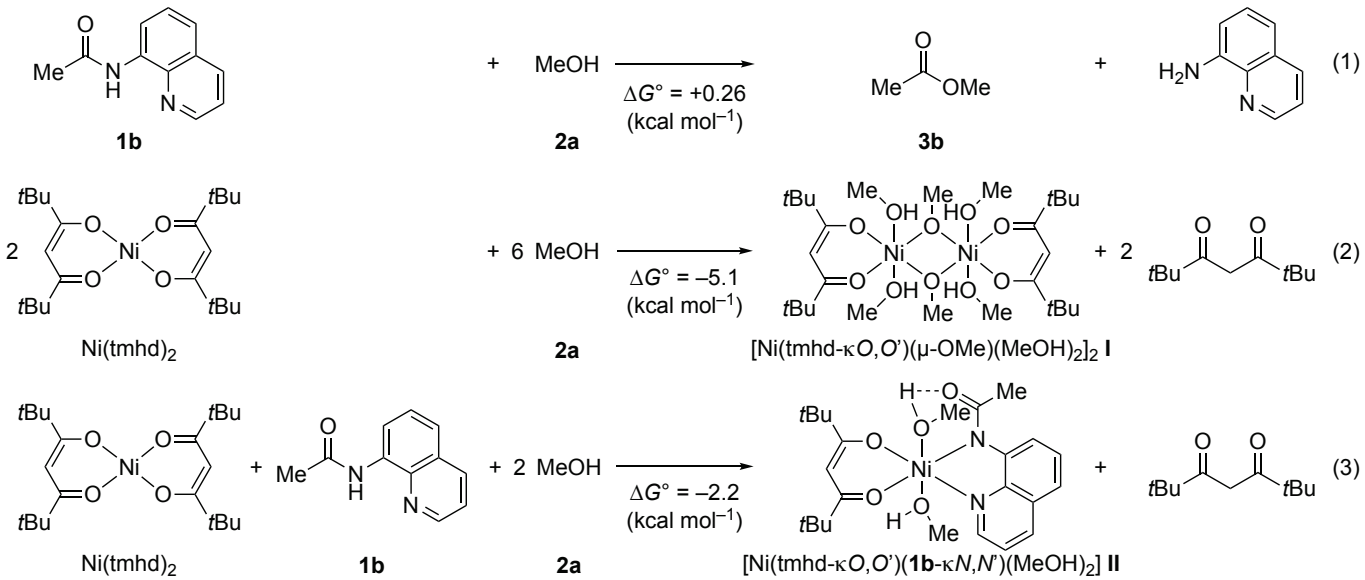

Scheme 3. Evaluation of the Reaction Thermodynamics by DFT Calculation

With the above computational results in hand, we next calculated the reaction pathway of the alcoholysis of 8-aminoquinoline amide **1b** catalyzed by $Ni(tmhd)_2$ (Scheme 4). Of note, all the Gibbs energies presented in Scheme 4 are relative to isolated species, such as $Ni(tmhd)_2$, **1b**, and **2a**. Because formation of the Ni complex **II** from Ni dimer **I** was thermodynamically feasible ($\Delta G°$ = +0.32 kcal mol^{-1}), Ni complex **II** was selected as the starting point. By considering the structure of Ni complex **II**, direct alcoholysis of 8-aminoquinoline amide from complex **II** seems to be difficult, and a proton transfer reaction from the coordinated MeOH to the amide nitrogen of **1b** was instead considered as the reaction pathway. In this case, the proton-transfer reaction from the oxygen atom to the nitrogen atom proceeded with a barrier of +14.5 kcal mol^{-1} via the transition state **II-TS** to give complex **III-H**. Complex **III-H** then dissociated the coordinated methanol to give complex **IV-H** without significant energy differences. Next, the methanol molecule in complex **IV-H** reacted with the 8-aminoquinoline amide via the six-membered ring transition state **IV-H-TS** with a barrier of +28.3 kcal mol^{-1}, producing tetrahedral intermediate **V-H** with an *N*,*N*,*O*-tridentate coordination to the nickel metal. From intermediate **V-H**, the C–N bond of the tetrahedral carbon dissociated to give complex **VI-H** via the transition state **V-H-TS**, with the highest transition state energy of +29.2 kcal mol^{-1} in the overall reaction pathway. After the release of ester **3b** and the association of **2a**, complex **VI-H** was converted to complex **VII-H** with octahedral coordination for the nickel atom, and complex **VII-H** had the lowest energy structure ($\Delta G°$ = –1.0 kcal mol^{-1}) along the reaction pathway. Next, a proton transfer from the coordinated MeOH to the anionic nitrogen, similar to the reaction from complex **II-H** to **III-H**, gave complex **VIII-H** via transition state **VII-H-TS**. From complex **VIII-H**, dissociation of the 8-aminoquinoline and association of **1b** gave complex **III′-H** with a Gibbs energy of +9.3 kcal mol^{-1}. The energy difference between the complex **III-H** and **III′-H** ($\Delta G°$ = –1.6 kcal mol^{-1}) is due to the thermodynamic energy differences between the starting materials (**1b** and **2a**) and the products (**3b** and 8-aminoquinoline) with the consideration of the concentration effects of MeOH (24.72 M).

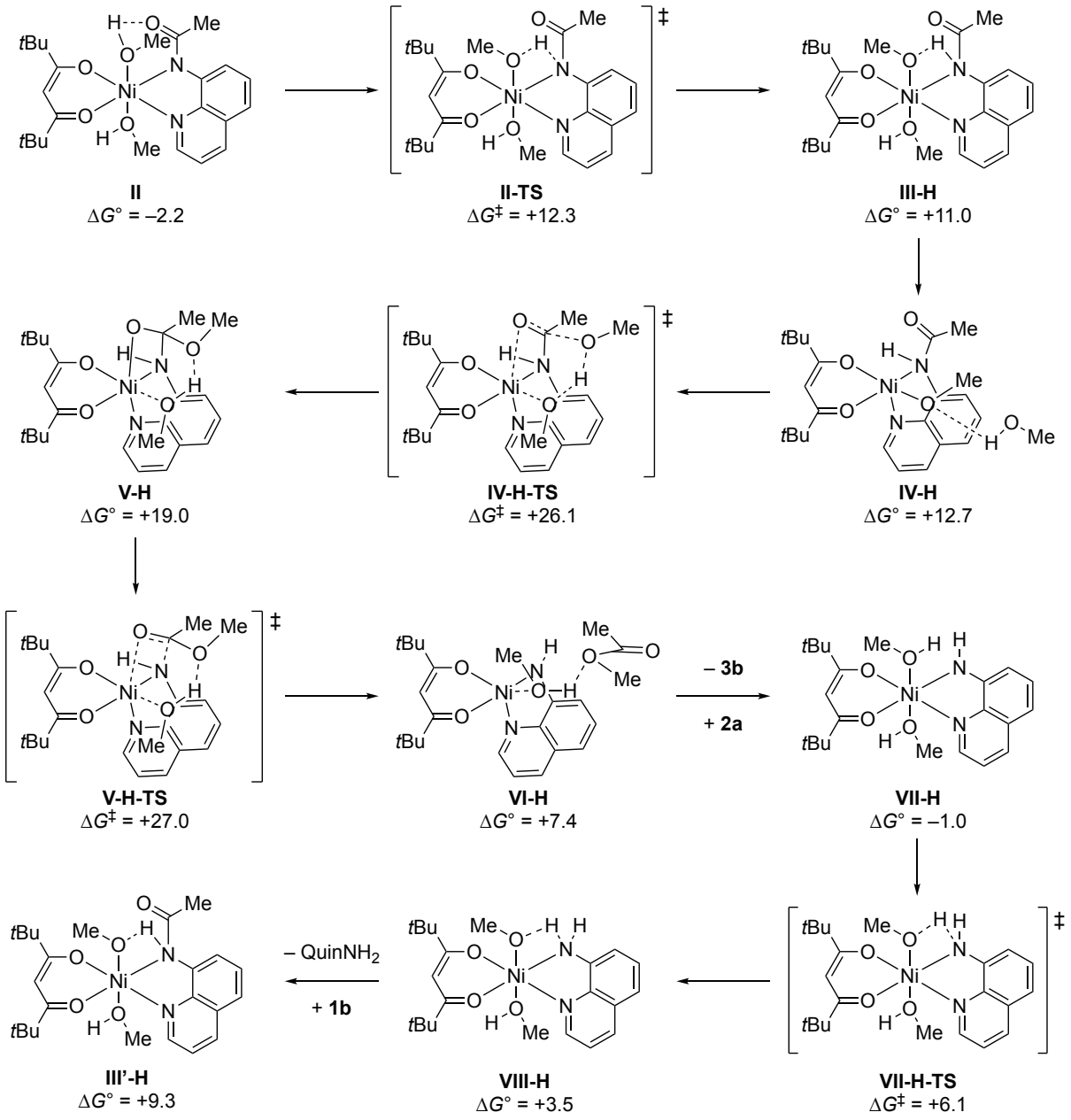

Scheme 4. DFT Calculation of the Reaction Pathway of the Nickel-Catalyzed Alcoholysis with *N*–H Amide **1b**

With the consideration of the above reaction pathway for *N*–H amide **1b**, we examined the similar reaction pathway with *N*-methylated 8-aminoquinoline amide **1c**, for which the previously proposed mechanism shown in Scheme 2 is inconsistent because the deprotonation of the N–H moiety is impossible. With the complex **III-Me** as the starting point, the reaction pathway in Scheme 4 was followed to give similar intermediates and transition states with reasonable activation energies (Scheme 5). These results indicate that the reaction pathway in Scheme 4 is also consistent with the experimental observations that the *N*-Me-substituted 8-aminoquinoline amide also reacted under the reaction conditions.

It is noted that the structure of **1c** in the complex **III-Me** is highly twisted with the deformation energy of +1.4 kcal mol^{-1} relative to the untwisted **1c**.

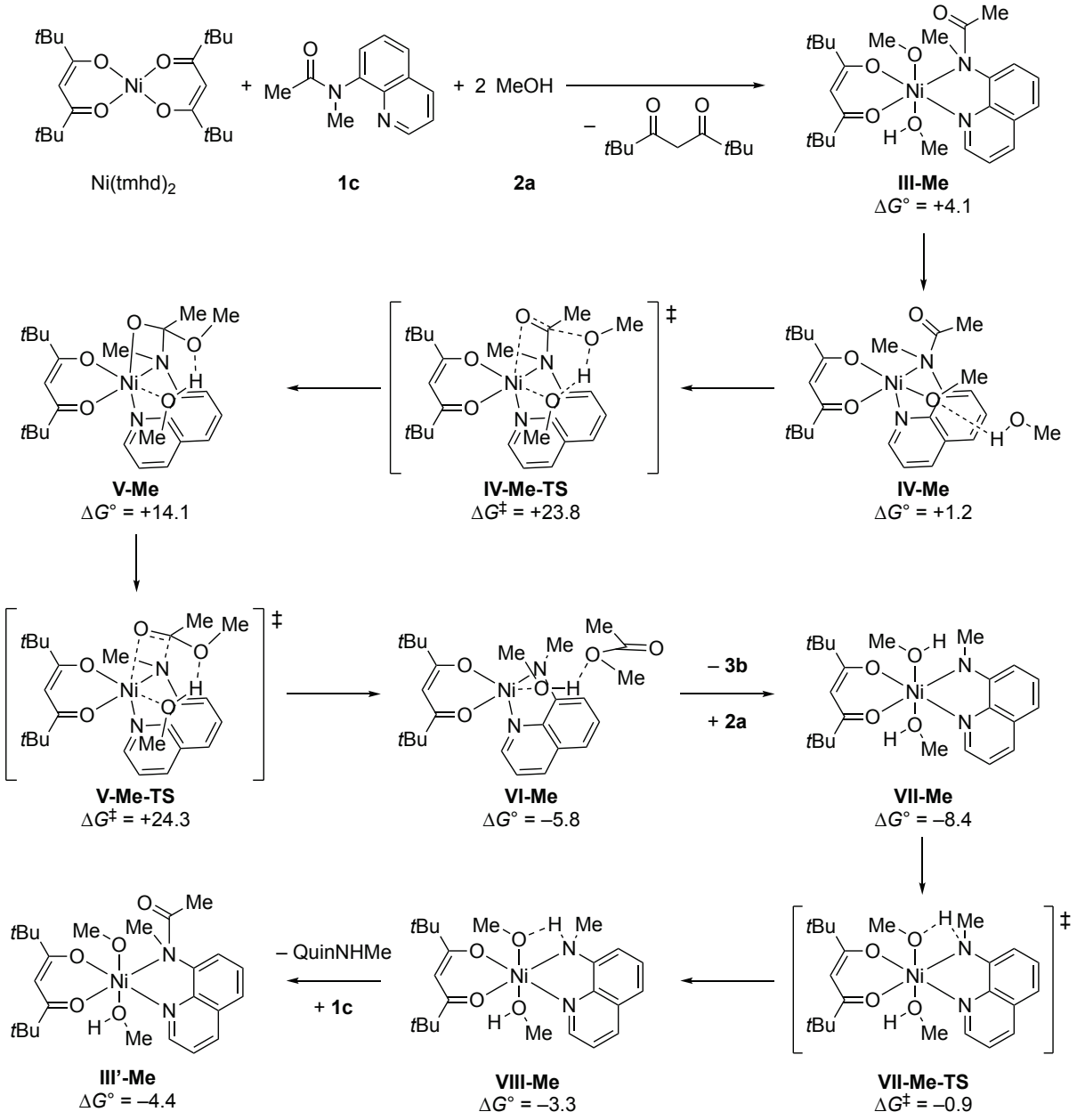

Scheme 5. DFT Calculation of the Reaction Pathway of the Nickel-Catalyzed Alcoholysis with *N*–Me Amide **1c**

On the basis of the information above, we propose the revised reaction mechanism of the nickel-catalyzed alcoholysis of 8-aminoquinoline amides as shown in Scheme 6. The reaction starts with the formation of dimeric nickel complex **I** that is more stable than the starting monomeric nickel complex Ni(tmhd)$_2$. Next, coordination of 8-aminoquinoline amide **1** provided monomeric nickel complex **II**, which is converted to the complex **III** via a proton transfer. The catalytic cycle then starts with the complex **III**, and the

addition of alcohol **2** proceeds via complex **IV** to give intermediate **V** with a tetrahedral carbon at the carbonyl group. Then C–N bond cleavage proceeds via the transition state **V-TS**, which the turnover-limiting step in the catalytic cycle. The produced complex **VI** releases the ester **3** to give complex **VII**, the resting state of the catalytic cycle. From the complex **VII**, a proton transfer gives complex **VIII**, and a ligand exchange provides the starting complex **III**, closing the catalytic cycle.

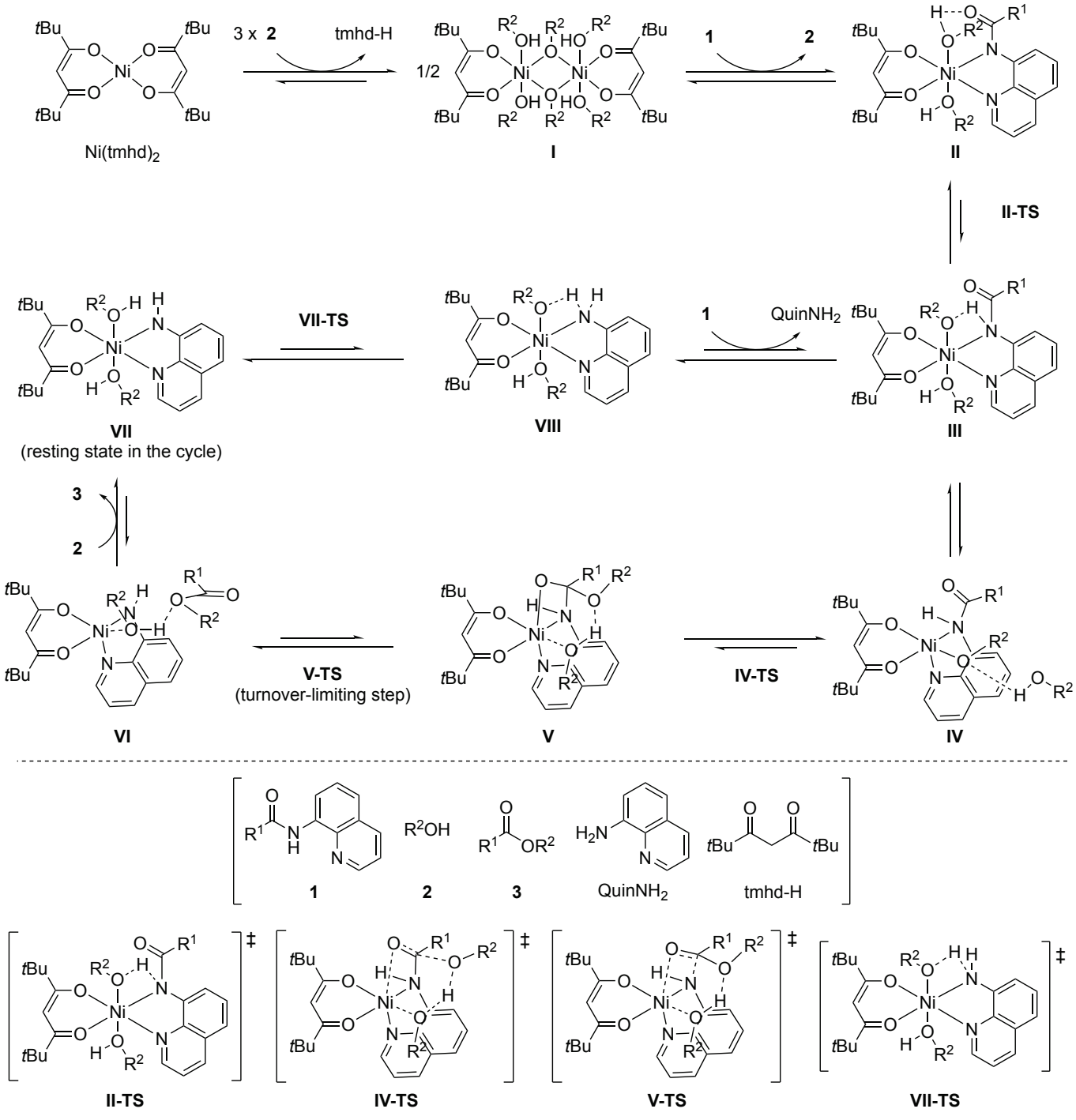

Scheme 6. Revised Proposed Mechanism

CONCLUSION

In conclusion, we reported the mechanistic studies of nickel-catalyzed direct alcoholysis of 8-aminoquinoline amides. First, kinetic experiments were performed to obtain the experimental evidence, and the results suggested that the nickel(II) catalyst had oligomeric form as the off-cycle species and that the 8-aminoquinoline amides coordinated to the nickel catalyst at the initial stage of the reaction. In addition, the addition of 8-aminoquinoline decelerated the reaction, suggesting that 8-aminoquinoline coordinated to the nickel(II) catalyst after the cleavage of amides. Next, DFT calculations were performed to clarify the detailed reaction mechanism, and our results showed that the calculated Gibbs energies were consistent with the experimental observations and that the reactions proceeded via the intermediate with *N*,*N*,*O*-tridentate coordination of 8-aminoquinoline amide moiety to the nickel(II) metal center. Furthermore, the alcoholysis reactions proceeded even without the deprotonation of the N–H bond of 8-aminoquinoline amides, as opposed to the proposed mechanism found in the C–H bond functionalization reactions of 8-aminoquinoline amides. We hope that our mechanistic studies described above could help the development of the related alcoholysis reactions in the future.

EXPERIMENTAL

General Experimental Details. All reactions were performed under an argon atmosphere using a Schlenk technique unless otherwise noted. All commercially available reagents and catalysts were used without further purification unless otherwise noted. Methanol (MeOH) was dried over molecular sieves before use. Nuclear magnetic resonance (NMR) spectra were acquired on a 500 MHz Bruker Avance III spectrometer.

Preparation of Starting Materials and Catalysts. All the starting materials and catalysts were prepared according to the previous procedure.[7]

General Procedure for the Kinetic Experiments. To a 4 mL vial with a Teflon-lined screw cap and a magnetic stir bar were added $Ni(tmhd)_2$, 8-aminoquinoline amide **1a** and MeOH (**2a**) under an argon atmosphere. After the cap was tightly closed, the mixture was stirred at 80 °C for the indicated time on a hot plate magnetic stirrer using an aluminum block. The sample was taken from the mixture at each time point and diluted with $CDCl_3$, and the yield of **3a** was determined by ^1H NMR analysis of the crude mixture.

General Procedure for the Computational Studies. The computational details were described in the text above. The optimized geometry and energies for each structure were summarized in the Supporting Information.

ACKNOWLEDGEMENTS

This paper is dedicated to Professor Kaoru Fuji on the occasion of his 80th birthday. This work was supported by Grant-in-Aid for Scientific Research on Innovative Areas (JSPS KAKENHI Grant No. JP15H05846 in Middle Molecular Strategy for T.O.) from JSPS, and Basis for Supporting Innovative Drug Discovery and Life Science Research (BINDS) (Grant Number JP18am0101091) from AMED, Uehara Memorial Foundation and Takeda Science Foundation. The computation was carried out using the computer resource offered under the category of General Projects by Research Institute for Information Technology, Kyushu University.

REFERENCES AND NOTES

1. For the reactivity of amides, see: W. Mabeyd and T. Mill, *J. Phys. Chem. Ref. Data*, 1978, **7**, 383; P. G. M. Wuts, Greene's Protective Groups in Organic Synthesis, 5th edn.; John Wiley & Sons: Hoboken, NJ, 2014; pp. 907 − 990 and 1116 − 1119. For the reactivity of alcohols, see: https://www.cup.lmu.de/oc/mayr/reaktionsdatenbank/ accessed on June 20, 2019.
2. For selected recent examples of alcoholysis of amides, see: M. C. Bröhmer, S. Mundinger, S. Bräse, and W. Bannwarth, *Angew. Chem. Int. Ed.*, 2011, **50**, 6175; M. Hutchby, C. E. Houlden, M. F. Haddow, S. N. G. Tyler, G. C. Lloyd-Jones, and K. I. Booker-Milburn, *Angew. Chem. Int. Ed.*, 2012, **51**, 548; S. M. A. H. Siddiki, A. S. Touchy, M. Tamura, and K.-i. Shimizu, *RSC Adv.*, 2014, **4**, 35803; C. Balachandra and N. K. Sharma, *Org. Lett.*, 2015, **17**, 3948; K. Yamada,Y. Karuo, Y. Tsukada, and M. Kunishima, *Chem. Eur. J.*, 2016, **22**, 14042; S. Adachi, N. Kumagai, and M. Shibasaki, *Chem. Sci.*, 2017, **8**, 85.
3. Y. Kita, Y. Nishii, T. Higuchi, and K. Mashima, *Angew. Chem. Int. Ed.*, 2012, **51**, 5723; Y. Kita, Y. Nishii, A. Onoue, and K. Mashima, *Adv. Synth. Catal.*, 2013, **355**, 3391; B. N. Atkinson and J. M. J. Williams, *Tetrahedron Lett.*, 2014, **55**, 6935; Y. Nishii, S. Akiyama, Y. Kita, and K. Mashima, *Synlett*, 2015, **26**, 1831; Y. Nishii, T. Hirai, S. Fernandez, P. Knochel, and K. Mashima, *Eur. J. Org. Chem.*, 2017, **2017**, 5010; H. Nagase, T. Hirai, D. Kato, S. Soma, S.-y. Akebi, and K. Mashima, *Chem. Sci.*, 2019, **10**, 2860.
4. L. Hie, N. F. F. Nathel, T. K. Shah, E. L. Baker, X. Hong, Y.-F. Yang, P. Liu, K. N. Houk, and N. K. Garg, *Nature*, 2015, **524**, 79; L. Hie, E. L. Baker, S. M. Anthony, J.-N. Desrosiers, C. Senanayake, and N. K. Garg, *Angew. Chem. Int. Ed.*, 2016, **55**, 15129; N. A. Weires, D. D. Caspi, and N. K. Garg, *ACS Catal.*, 2017, **7**, 4381.
5. For selected reviews on directing group amides, see: G. Rouquet and N. Chatani, *Angew. Chem. Int. Ed.*, 2013, **52**, 11726; O. Daugulis, J. Roane, and L. D. Tran, *Acc. Chem. Res.*, 2015, **48**, 1053; L. C.

Misal Castro and N. Chatani, *Chem. Lett.*, 2015, **44**, 410; J. Liu, G. Chen, and Z. Tan, *Adv. Synth. Catal.*, 2016, **358**, 1174.

6. Y. Shimizu, H. Morimoto, M. Zhang, and T. Ohshima, *Angew. Chem. Int. Ed.*, 2012, **51**, 8564; Y. Shimizu, M. Noshita, Y. Mukai, H. Morimoto, and T. Ohshima, *Chem. Commun.*, 2014, **50**, 12623; M. Noshita, Y. Shimizu, H. Morimoto, and T. Ohshima, *Org. Lett.*, 2016, **18**, 6062; M. Noshita, Y. Shimizu, H. Morimoto, S. Akai, Y. Hamashima, N. Ohneda, H. Odajima, and T. Ohshima, *Org. Process Res. Dev.*, 2019, **23**, 588.
7. T. Deguchi, H.-L. Xin, H. Morimoto, and T. Ohshima, *ACS Catal.*, 2017, **7**, 3157.
8. For selected examples, see: D. Shabashov and O. Daugulis, *J. Am. Chem. Soc.*, 2010, **132**, 3965; Q. Gou, Z.-F. Zhang, Z.-C. Liu, and J. Qin, *J. Org. Chem.*, 2015, **80**, 3176; R. Shang, L. Ilies, S. Asako, and E. Nakamura, *J. Am. Chem. Soc.*, 2014, **136**, 14349; B. K. Singh and R. Jana, *J. Org. Chem.*, 2016, **81**, 831; M. D. Reddy and E. B. Watkins, *J. Org. Chem.*, 2015, **80**, 11447; Y. Ano, M. Tobisu, and N. Chatani, *J. Am. Chem. Soc.*, 2011, **133**, 12984; J. A. Gurak, Jr., K. S. Yang, Z. Liu, and K. M. Engle, *J. Am. Chem. Soc.*, 2016, **138**, 5805. For selected examples using our Ni-catalyzed conditions after our publication, see: T. Zeng, Z. Liu, M. A. Schmidt, M. D. Eastgate, and K. M. Engle, *Org. Lett.*, 2018, **20**, 3853; H. Wang, Z. Bai, T. Jiao, Z. Deng, H. Tong, G. He, Q. Peng, and G. Chen, *J. Am. Chem. Soc.*, 2018, **140**, 3542; M. Liu, P. Yang, M. K. Karunananda, Y. Wang, P. Liu, and K. M. Engle, *J. Am. Chem. Soc.*, 2018, **140**, 5805; J. Derosa, V. A. van der Puyl, V. T. Tran, M. Liu, and K. M. Engle, *Chem. Sci.*, 2018, **9**, 5278; V. A. van der Puyl, J. Derosa, and K. M. Angle, *ACS Catal.*, 2019, **9**, 224; H.-C. Shen, L. Zhang, S.-S. Chen, J. Feng, B.-W. Zhang, Y. Zhang, X. Zhang, Y.-D. Wu, and L.-Z. Gong, *ACS Catal.*, 2019, **9**, 791; S. K. Nimmagadda, M. Liu, M. K. Karunananda, D.-W. Gao, O. Apolinar, J. S. Chen, P. Liu, and K. M. Engle, *Angew. Chem. Int. Ed.*, 2019, **58**, 3923.
9. J. Burés, *Angew. Chem., Int. Ed.*, 2016, **55**, 2028; J. Burés, *Angew. Chem., Int. Ed.*, 2016, **55**, 16084.
10. D. G. Blackmond, *Angew. Chem. Int. Ed.*, 2005, **44**, 4302; J. S. Mathew, M. Klussmann, H. Iwamura, F. Valera, A. Futran, E. A. C. Emanuelsson, and D. G. Blackmond, *J. Org. Chem.*, 2006, **71**, 4711; D. G. Blackmond, *J. Am. Chem. Soc.*, 2015, **137**, 10852. Although the original same [*e*] experiments use the difference of the initial concentration of two reactants A and B ($[e] = [A]_0 - [B]_0$), we assumed that the difference of concentration of two reactants in this reaction was essentially same in all the cases because the large excess amounts of one reactant is used ($[e] = [MeOH]_0 - [\mathbf{1a}]_0 = 24.6$, 24.5, and 24.2 (M) for $[\mathbf{1a}]_0 = 0.125$, 0.25, and 0.50 (M), respectively), and the small concentration difference would only marginally affect the reaction rate. Therefore, we call the present reaction conditions as the pseudo-same [*e*] conditions in this manuscript.

11. R. D. Baxter, D. Sale, K. M. Engle, J.-Q. Yu, and D. G. Blackmond, *J. Am. Chem. Soc*., 2012, **134**, 4600.
12. Gaussian 16, Revision A.03, M. J. Frisch, G. W. Trucks, H. B. Schlegel, G. E. Scuseria, M. A. Robb, J. R. Cheeseman, G. Scalmani, V. Barone, G. A. Petersson, H. Nakatsuji, X. Li, M. Caricato, A. V. Marenich, J. Bloino, B. G. Janesko, R. Gomperts, B. Mennucci, H. P. Hratchian, J. V. Ortiz, A. F. Izmaylov, J. L. Sonnenberg, D. Williams-Young, F. Ding, F. Lipparini, F. Egidi, J. Goings, B. Peng, A. Petrone, T. Henderson, D. Ranasinghe, V. G. Zakrzewski, J. Gao, N. Rega, G. Zheng, W. Liang, M. Hada, M. Ehara, K. Toyota, R. Fukuda, J. Hasegawa, M. Ishida, T. Nakajima, Y. Honda, O. Kitao, H. Nakai, T. Vreven, K. Throssell, J. A. Montgomery, Jr., J. E. Peralta, F. Ogliaro, M. J. Bearpark, J. J. Heyd, E. N. Brothers, K. N. Kudin, V. N. Staroverov, T. A. Keith, R. Kobayashi, J. Normand, K. Raghavachari, A. P. Rendell, J. C. Burant, S. S. Iyengar, J. Tomasi, M. Cossi, J. M. Millam, M. Klene, C. Adamo, R. Cammi, J. W. Ochterski, R. L. Martin, K. Morokuma, O. Farkas, J. B. Foresman, and D. J. Fox, Gaussian, Inc., Wallingford CT, 2016.
13. A. D. Becke, *J. Chem. Phys*., 1993, **98**, 5648; C. Lee, W. Yang, and R. G. Parr, *Phys. Rev. B*, 1988, **37**, 785; S. H. Vosko, L. Wilk, and M. Nusair, *Can. J. Phys*., 1980, **58**, 1200.
14. J. B. Foresman and Æ Frisch, in Exploring Chemistry with Electronic Structure Methods, Third Edition, Gaussian Inc., pp. 108–109.
15. P. L. da Silva, L. Guimarães, and J. R. Pliego, Jr., *J. Phys. Chem. B*, 2013, **117**, 6487.
16. Y. Zhao and D. G. Truhlar, *Theor. Chem. Acc*., 2008, **120**, 215.
17. A. V. Marenich, C. J. Cramer, and D. G. Truhlar, *J. Phys. Chem. B*, 2009, **133**, 6378.
18. We also calculated the cases where the dimeric Ni complexes are the active species and a tetrameric Ni species is the resting state, but the calculated Gibbs energy for the activation was more than 40 kcal mol^{-1}, which is difficult to overcome under the reaction conditions.